CDF NOTE 10799

A Search for the Standard Model Higgs Boson in the Process $ZH \to \ell^+\ell^- b\bar{b}$ Using 9.45 fb^{-1} of CDF II Data

The CDF Collaboration
http://www-cdf.fnal.gov
(Dated: March 7, 2012)

We present the results of a search for the standard model (SM) Higgs boson in the associated production process $p\overline{p} \to ZH \to \ell^+\ell^- b\bar{b}$. We analyze a sample of Tevatron $p\overline{p}$ collisions at $\sqrt{s}$=1.96 TeV, corresponding to an integrated luminosity of 9.45 fb^{-1}, and collected by the CDF II detector. In events with two electron (e) or two muon (μ) candidates and 2 or 3 energetic jets, at least one of which is identified as a bottom-quark (b) jet, we set 95% confidence level upper limits on the associated Higgs production cross section (σ_{ZH}) times the branching ratio (BR) of $H \to b\bar{b}$ for thirteen Higgs boson mass hypotheses between 90 GeV/c^2 and 150 GeV/c^2. For a Higgs boson mass of 115 GeV/c^2, we observe (expect) an upper limit of 4.7 (2.6) times the SM value of $\sigma_{ZH} \times BR(H \to b\bar{b})$.

Preliminary Results for Winter 2012 Conferences

I. INTRODUCTION

The mechanism of spontaneous electroweak symmetry breaking (EWSB) has yet to be resolved in the standard model of particle physics (SM). In the most simple formulation, EWSB is achieved through the introduction of the theoretical Higgs field [1–3], and consequently predicts the existence of the unobserved Higgs boson. Precision electroweak measurements constrain the mass of the Higgs boson (M_H) to be less than 152 GeV/c^2 at the 95% confidence level [4]. Previous searches at LEP, the Tevatron, and LHC have excluded masses below 115.5 GeV/c^2 and between 127 GeV/c^2 and 600 GeV/c^2 [5–8] respectively.

A Higgs boson with a mass of 127 GeV/c^2 or less will decay to a bottom quark pair ($b\bar{b}$) approximately 80% of the time [9]. While the rate of associated ZH production is small ($\sim 0.1\ pb$), the decay products of the associated Z boson (here, e^+e^- or $\mu^+\mu^-$) serve to distinguish the $H \to b\bar{b}$ decay from multi-jet production, making $ZH \to \ell^+\ell^- b\bar{b}$ a viable Tevatron search mode.

In this note, we present an updated search for $ZH \to \ell^+\ell^- b\bar{b}$ in which we expand upon the techniques of previous searches performed in 4.1 fb^{-1} [10] and in 7.5-7.9 fb^{-1}[11, 12]. This search incorporates new multivariate b-jet identification and updated multi-stage artificial neural network (NN) background discrimination. These modification to the analysis technique and the expanded data set result in up to a 34% improvement in sensitivity to a Higgs boson signal. In addition we expand the search to consider a Higgs boson with a mass of less than 100 GeV/c^2 for the first time.

This note is structured as follows: Section II describes the initial (trigger) online event selection and the data sample considered. Section III details the selections used to identify a sample of candidate events consistent with the expected topology of the $ZH \to \ell^+\ell^- b\bar{b}$ process. The composition of our selected sample, simulation of ZH signal, and the formulation of our data model are discussed in Section IV. We utilize a neural network to correct the energy of jets in candidate events, this correction is described in Section V. The training and construction of our NN event discriminants are detailed in Section VI. The extraction of upper limits on the value of $\sigma_{ZH} \times BR(H \to b\bar{b})$ is presented in VIII.

II. DATA SAMPLE & ONLINE EVENT SELECTION

The data used in this search was collected by the upgraded CDF II detector, between February 2002 and September of 2011, and corresponds to 9.45 fb^{-1} of Tevatron $p\overline{p}$ collisions at $\sqrt{s}$=1.96 TeV. The CDF II detector is described in detail elsewhere [13] and consists of tracking systems immersed in a 1.4 T magnetic field, surrounded by calorimetery that provides coverage for $|\eta| < 3.6$ [14]. A system of drift chambers external to the calorimetery provides muon detection capability for $|\eta| < 1.5$. CDF II records only those collision events which meet the criteria of a multi-level online event selection (trigger) system.

In this search, we utilize data selected by one of three sets of trigger algorithms. The first set consists of algorithms which require events to possess one or two electron candidates. The candidates are required to have a minimum transverse energy (E_T) of 8 to 18 GeV, varying based on the specific algorithm. Algorithms which require a pair of electron candidates further require a reconstructed dielectric candidate mass of greater than 40 GeV/c^2. The second set of trigger algorithms requires the presence of a muon candidate with a minimum transverse momentum (p_T) of 18 to 22 GeV, again varying based on the specific algorithm. The third group of algorithms accepts events with significant missing transverse energy ($\not\!\!E_T$) [15], generally above 30 GeV. Several of these algorithms impose additional requirements on the number (typically 2) and transverse energy (generally greater than 10 GeV) of jets in the event.

III. EVENT SELECTION

We impose additional requirements on the events selected by our trigger algorithms to remove events that are inconsistent with the $ZH \to \ell^+\ell^- b\bar{b}$ signal. We begin by rejecting events that were recorded without operational calorimeter, tracking or silicon vertex detectors. We further remove events that are not well contained in the detector (*i.e.* those with a primary interaction vertex located more than 60 cm from the center of CDF II), and events that are likely to have originated from non-collison sources (primarily cosmic rays).

We require a $Z \to \ell^+\ell^-$ candidate to be present in each event. We form candidate Z bosons from pairs of electron or muon candidates selected by a combination of multivariate algorithms and various requirements on detector signatures including calorimeter energy, track momentum and pseudo-rapidity (η). These requirements and algorithms are unchanged from those used in the previous version of this search and are described in Refs. [11, 12]. We impose an opposite charge requirement on all $Z \to \ell^+\ell^-$ candidates when both constituent leptons are muons, or are electrons

with $|\eta| < 1.1$. We remove events in which the reconstructed Z boson has a mass of less than 76 or greater than 106 GeV/c^2.

In addition to a $Z \to \ell^+\ell^-$ candidate, we require events to contain a candidate $H \to b\bar{b}$ decay. To reconstruct $H \to b\bar{b}$ candidates, we identify jets using a cone algorithm [16] which combines calorimeter energy deposits to form jets with a radius of 0.4 in η-ϕ space. Jet energies include corrections for regional variations in calorimeter response and instrumentation, and the energy contribution from additional $p\overline{p}$ interactions. We retain events with two or three jets with $|\eta| \leq 2.0$ and an E_T of greater than 25 GeV. Events in which the combined mass of the leading and second jet (as ranked in E_T) is less than 25 GeV/c^2 are removed.

We find 19302 events which pass the above selections. As these events contain $ZH \to \ell^+\ell^- b\bar{b}$ candidates prior to the requirement of consistency between the jets and b-quarks (*i.e.* before "b-tagging"), we designate these events as the "PreTag" sample.

We perform the analysis in a subset of the PreTag sample which consists of events with at least one b-tagged jet. We employ a new multivariate b-tagging algorithm specifically designed to increase the b-tag efficiency and reduce the frequency of incorrectly tagged $udsg$-jets (mistags) in CDF $H \to b\bar{b}$ searches. The Higgs-Optimized b-Identification Tagger (HOBIT) is a neural network b-jet tagging algorithm designed to identify b-jets from the decay of Higgs bosons. HOBIT is described in Ref. [17]. HOBIT combines quantities describing a jet's displaced vertices, tracks, and energy to return a numerical value. This analysis classifies a jet as having a "tight" b-tag if the HOBIT algorithm returns a value greater than 0.98. Similarly "loose" b-tags are defined by a HOBIT value between 0.72 and 0.98.

We form four categories of events with b-tagged jets. Events with two or more jets with tight b-tags comprise the "double-tight" (TT) category. Events with one jet with a tight b-tag and one or more jets with a loose b-tag form the "tight+loose" (TL) category. Those with one jet with a tight b-tag, and no other tight or loose b-tagged jets make up the "single tight" (Tx) category. Events with two or more jets with loose b-tags comprise the "double-loose" (LL) category. If a data event satisfies more than one tag category, then the *best* category is chosen, using the listed ordering.

The tag categories are subject to different systematic uncertainties, background compositions, and predicted ZH fractions, and are therefore maintained as separate analysis channels. Similarly we maintain $Z \to e^+e^-$ and $Z \to \mu^+\mu^-$ as separate analysis channels, and maintain a division between two and three jet events. In total we have 16 channels formed by 4 b-tag categories $\times$ 2 $Z \to \ell^+\ell^-$ types $\times$ 2 jet multiplicities. The 16 channels are simultaneously examined for ZH content and jointly used to set upper limits on $\sigma_{ZH} \times BR(H \to b\bar{b})$.

IV. DATA MODEL

Background processes possessing a detector signature similar to the signal are mainly those which contain two leptons and two (or more) jets in the final state. The dominant background is $Z + jets$, with Z + light flavor ($udsg$) jets forming the major background component before b-tag requirements are imposed. $Z + jets$ events are modeled using ALPGEN [18] with PYTHIA [19] for particle showering and hadronization. Signal, diboson (ZZ, WZ, WW), and $t\bar{t}$ processes are modeled with PYTHIA. The $t\bar{t}$ simulation assumes a top mass of 172.5 GeV/c^2. The assumed production rates for simulated background processes, and the SM values of σ_{ZH} and BR($H \to b\bar{b}$) are presented in Ref. [20].

We apply several corrections to the normalization of simulated samples to improve the agreement between the observed data and the model. We correct the luminosity profile of the simulated samples to match that observed in data. We correct the energy (1%) of observed leptons to ensure agreement with the energy distributions measured in data. In addition, we apply factors which correct for differences in lepton and b-jet reconstruction and selection efficiencies. To account for the selection efficiency of the CDF II trigger system, we employ multivariate trigger emulation. A neural network is trained to reproduce the combined trigger decision of the trigger detailed above. The output of this NN is applied to the model as an additional normalization factor on a per-event basis, and accurately reflects the probability of selection by the relevant triggers. Simulated c and b-quark processes are re-weighted to eliminate differences in the performance of the HOBIT algorithm between data and simulated samples. The simulated Z+light flavor (l.f.) jet samples are re-normalized based on the probability of the jets to satisfy the TT, TL, Tx, or LL selections. The derivation of the b-tag (and mistag) corrections are described in Ref. [17].

We account for the contribution of QCD multijet and W boson + jet backgrounds using a data-derived model for "misidentified" $Z \to \ell^+\ell^-$ candidates. For misidentified $Z \to e^+e^-$ candidates, we utilize a sample of events containing a single electron and and 3 or 4 jets. Each electron-jet pair in these events contributes to the misidentified $Z \to e^+e^-$ model with a weight reflecting the probability of the jet to be misidentified as an electron. The determination of the weights is described in Ref. [11]. The misidentified $Z \to \mu^+\mu^-$ contribution is modeled using like-sign muon pairs.

Inputs to the NN jet-energy correction algorithm
lead jet E_T
lead jet η
$\Delta\phi(\vec{\not\!\!E}_T,$ lead jet)
Z projection onto the lead jet
$\vec{\not\!\!E}_T$ projection onto the lead jet
second jet E_T
second jet η
$\Delta\phi(\vec{\not\!\!E}_T,$ second jet)
Z projection onto the second jet
$\vec{\not\!\!E}_T$ projection onto the second jet
$\not\!\!E_T$
$\Delta\phi$(lead jet, second jet)
number of jets

TABLE I: Inputs to the jet-energy correction neural network.

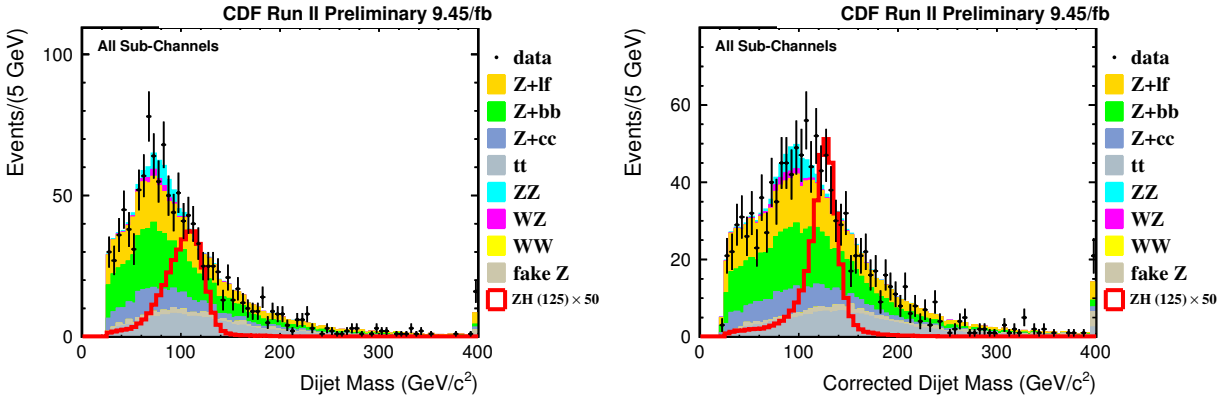

FIG. 1: The dijet invariant mass distribution for all b-tagged candidates before (left) and after (right) NN correction. The bin at 400 GeV/c^2 contains the histogram overflow.

V. NEURAL NETWORK JET ENERGY CORRECTION

To improve the separation of ZH signal from background, we utilize several multivariate techniques that use kinematic quantities as inputs. The dijet mass (M_{jj}) is one of the most useful quantities, with its separating power limited mainly by the jet-energy resolution. In ZH signal events with $Z \to \ell^+\ell^-$ incorrect measurement of jet energies results in apparent missing transverse energy $\vec{\not\!\!E}_T$. We correct jet energies, based upon the $\vec{\not\!\!E}_T$, and thereby improve the resolution on the dijet invariant mass. Jet-energy correction factors are computed by a NN trained to match measured jet energies to parton-level energies in Z+jets and signal events. Inputs to the NN are listed in Table I. The effect of the NN corrections on the reconstructed $H \to b\bar{b}$ mass is shown in Fig. 1. In b-tagged signal the resolution [21] on M_H is improved from about 18% to 11%.

VI. EVENT DISCRIMINANTS

We utilize new multivariate algorithms to improve our ability to distinguish between ZH signal and background processes. To isolate ZH signal from $t\bar{t}$ we employ an "expert" NN, trained to distinguish ZH from top. Similarly we use a second expert network to separate ZH from $Z + l.f.$ and Z+$c\bar{c}$ backgrounds. The expert networks have been re-optimized since the previous analysis [11, 12], with the most significant difference being that the $Z + l.f./Z$+$c\bar{c}$

Inputs to the expert neural networks		
$t\bar{t}$ Expert	$Z+l.f./Z+c\bar{c}$ Expert	WZ/ZZ Expert
$\not\!\!E_T$	NN Corrected M_{jj}	NN Corrected M_{jj}
$\vec{\not\!\!E}_T$ projection onto the all jets	2nd jet E_T	2nd jet E_T
E_T of Z+all jets	H_T [23]	$\cos(\theta^*)$ [24]
$\vec{\not\!\!E}_T$ projection onto the lead jet	$\Delta R(Z,$ jet 1)	$\Delta R(Z,$ jet 1)
E_T of Z+H candidates	combined mass of Z and all jets	$\Delta R(Z,\ H)$
$\vec{\not\!\!E}_T$ projection onto the 2nd jet	combined mass of Z and H candidates	H_T
$\Delta R(Z,$ all jets) [22]	ΔR(lepton 1, lepton 2)	Z projection onto all jets
NN Corrected M_{jj}	Z projection onto all jets	ΔR(lepton 1, lepton 2)
	Z p_T	Z p_T
	$\vec{\not\!\!E}_T$ projection onto all jets	
	jet 1 E_T	

TABLE II: Inputs to the expert neural networks, listed in descending order of importance.

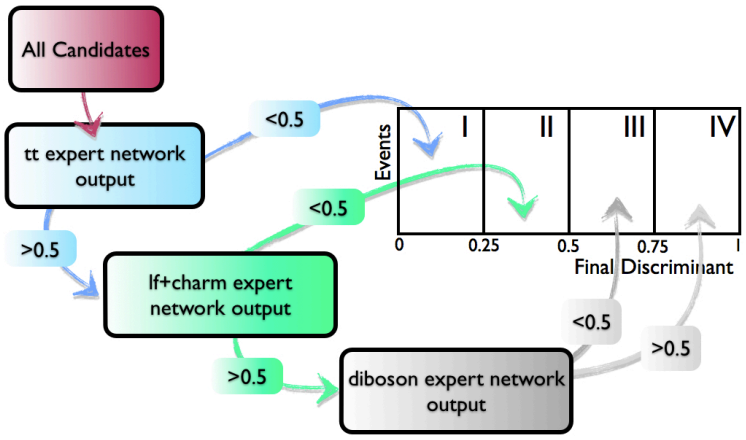

FIG. 2: Summary of the logic used to assign events to a region (I,II,II,IV) of the final discriminant.

expert replaces the b-jet flavor separator [25] used previously. For this analysis, we introduce a third expert network trained to distinguish ZZ and WZ from ZH signal. The input variables to each of the expert networks are listed in Table II.

We utilize the three expert networks to assign events to one of four distinct regions (labeled I,II, III, IV) in the final event discriminant used in the extraction of upper limits. If the $t\bar{t}$ expert returns a value of less than 0.5, the event is assigned to region I. Otherwise, if the $Z+l.f./Z+c\bar{c}$ expert returns a score of less than 0.5, the event is assigned to region II. If greater than 0.5, the event is passed through the diboson expert, and if the diboson expert returns a value less (greater) than 0.5, the event is assigned to region III (IV). The logic of region assignment is outlined in Figure 2. We validate the ability of our model to reproduce the observed shape of the expert discriminants in the PreTag sample. Expert network output for the model is compared to the PreTag data in Fig. 3.

In addition to the three expert neural networks, an additional network is trained to simultaneously separate ZH signal from all backgrounds. We employ 26 versions of this NN (designated "final discriminants"), optimized for different values of M_H and separately for 2 and 3 jet events. Once an event receives a region classification, it is evaluated by the final discriminant and assigned to a bin corresponding to the final discriminant score within the region. The inputs to the final discriminants are listed in Table III, while output for the model is compared to the

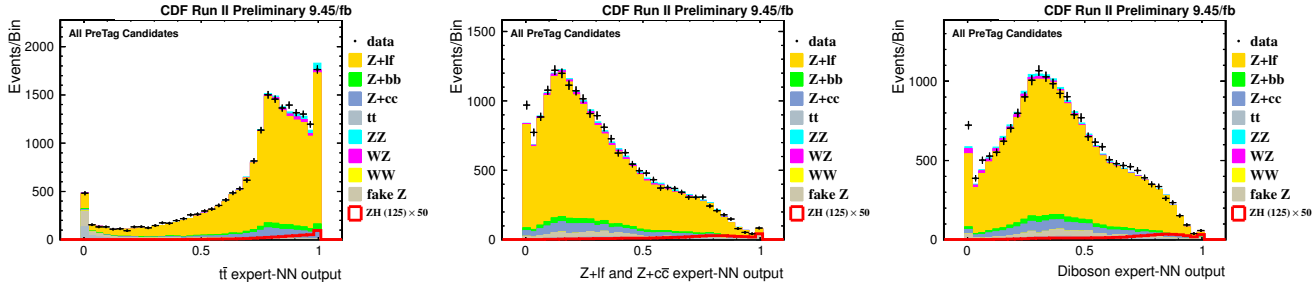

FIG. 3: Output of the expert discriminants in the PreTag (defined in text) sample. The bin at zero (one) contains the histogram underflow (overflow).

Inputs to the expert neural networks	
two jet final discriminant	three jet final discriminant
NN Corrected M_{jj}	NN Corrected M_{jj}
E_T of jet 1	Z projection onto all jets
$\Delta R(Z,\ H)$	$\vec{\not\!\!E}_T$ projection onto all jets
Z projection onto all jets	Z p_T
$\vec{\not\!\!E}_T$ projection onto all jets	$\vec{\not\!\!E}_T$ projection onto jet 1
ΔR(lepton 1, lepton 2)	ΔR(lepton 1, lepton 2)
$\cos(\theta^*)$ [24]	$\not\!\!E_T$
Z p_T	$\Delta R(Z,\ H)$
H_T [23]	$\vec{\not\!\!E}_T$ projection onto jet 2
E_T of jet 2	ΔR(jet 1, jet 2)
$\Delta R(Z,$ jet 1)	$\Delta R(Z,$ jet 1)
$\vec{\not\!\!E}_T$ projection onto jet 1	$\cos(\theta^*)$
$\Delta R(Z,\ jet2)$	

TABLE III: Inputs to the expert neural networks, listed in descending order of importance.

PreTag data in Fig. 4.

VII. SYSTEMATICS

We account for the effect of uncertainties on the measurement of the integrated luminosity, lepton reconstruction efficiencies, measurement of lepton energy/momentum, normalization of the misidentified $Z \to \ell^+\ell^-$ backgrounds, mistag probabilities, b-tag rate, production cross sections, and the trigger parameterization and the amount of additional initial or final state radiation (ISR/FSR). We assume a 5% uncertainty on the value of σ_{ZH}. In addition we evaluate the effect of uncertainty in the measurement of the jet energy scale (JES) on both the normalization and the shape of final discriminant output. The largest impact on sensitivity is due to uncertainties on the b-tag rate. In combination systematic uncertainties degrade sensitivity to a ZH signal by approximately 13%. Appendix X summarize the systematic uncertainties applied in our limit calculations. Detailed descriptions of the systematic uncertainties are provided in Refs. [11, 12, 17].

VIII. RESULTS

After applying b-tagging, our final event totals are shown in Tables IV and V. The neural net output distributions for the signal region are shown in Figures 5 and 6. We do not observe a significant excess over the number of events predicted by our background model, and proceed to quantify the maximum allowed ZH contamination in the

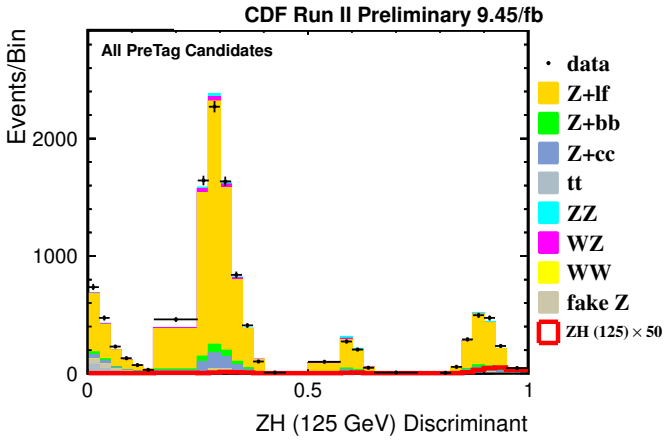

FIG. 4: Output of the final discriminants optimized for a 125 GeV/c^2 Higgs boson in the PreTag (defined in text) sample. We choose a variable bin-width to maintain sufficient statistics in each bin.

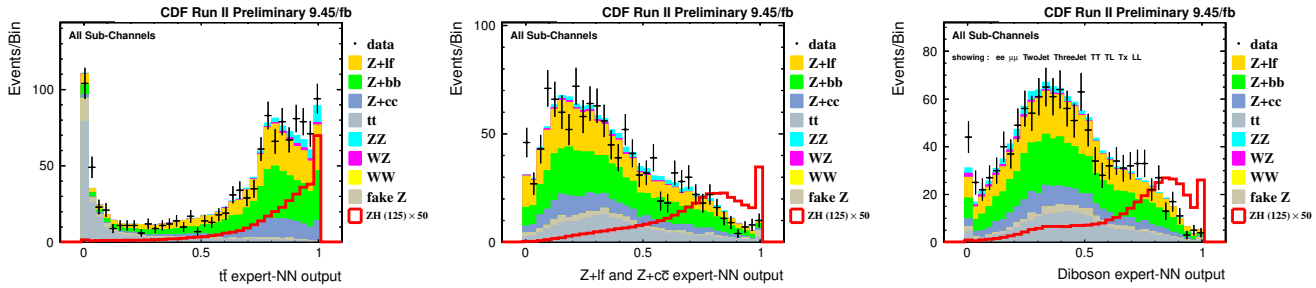

FIG. 5: Output of the expert discriminants in the b-tagged (defined in text) sample. The bin at zero (one) contains the histogram underflow (overflow).

data. We use the MCLIMIT [26] machinery for this, and do a binned fit of the neural net distribution, including systematics. We set 95% confidence level upper limits on $\sigma_{ZH} \times BR(H \to b\bar{b})$ and compute observed limits for Higgs masses between 90 and 150 GeV/c^2 in 5 GeV intervals. The results are shown in Table VI and Figure 7.

IX. CONCLUSIONS

We have evaluated a new limit with an updated dataset larger than in the previous analysis. We have calculated a 95% confidence level upper limits from 1.0 to 36.5 times the Standard Model prediction for Higgs Boson masses between 90 GeV/c^2 to 150 GeV/c^2. For a Standard Model Higgs boson mass of 120 GeV, we find the expected 95% confidence level upper limit to be 3.1 times the Standard Model prediction with an observed limit of 5.7.

Acknowledgments

We thank the Fermilab staff and the technical staffs of the participating institutions for their vital contributions. This work was supported by the U.S. Department of Energy and National Science Foundation; the Italian Istituto Nazionale di Fisica Nucleare; the Ministry of Education, Culture, Sports, Science and Technology of Japan; the Natural Sciences and Engineering Research Council of Canada; the National Science Council of the Republic of China; the Swiss National Science Foundation; the A.P. Sloan Foundation; the Bundesministerium fuer Bildung und Forschung, Germany; the Korean Science and Engineering Foundation and the Korean Research Foundation; the Particle Physics and Astronomy Research Council and the Royal Society, UK; the Russian Foundation for Basic Research; the Comision Interministerial de Ciencia y Tecnologia, Spain; and in part by the European Community's Human Potential Programme under contract HPRN-CT-20002, Probe for New Physics.

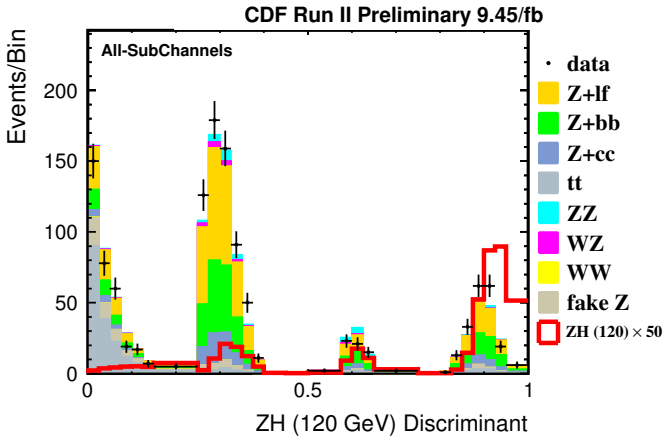

FIG. 6: Output of the final discriminants optimized for a 120 GeV/c^2 Higgs boson in the b-tagged (defined in text) sample. We choose a variable bin-width to maintain sufficient statistics in each bin.

	–Two Jets–				–Three Jets–			
Process	TT	TL	Tx	LL	TT	TL	Tx	LL
$t\bar{t}$	20.1 ± 2.8	21.5 ± 2.8	36.1 ± 4.7	6.1 ± 0.8	7.5 ± 1.2	9.3 ± 1.4	13.5 ± 1.9	2.9 ± 0.5
Diboson	4.7 ± 0.6	6.5 ± 0.9	19.6 ± 1.8	3.9 ± 0.4	0.7 ± 0.1	1.3 ± 0.2	3.0 ± 0.4	1.0 ± 0.1
$Z + b\bar{b}$	19.1 ± 8.0	26.8 ± 11.3	81.5 ± 34.2	10.2 ± 4.4	4.5 ± 2.0	6.5 ± 2.9	14.1 ± 6.2	2.5 ± 1.1
$Z + c\bar{c}$	1.5 ± 0.6	6.9 ± 2.9	39.0 ± 16.8	7.3 ± 3.1	0.5 ± 0.2	1.7 ± 0.8	7.4 ± 3.3	2.4 ± 1.1
$Z + l.f.$	0.7 ± 0.3	8.3 ± 2.0	124.9 ± 27.5	27.5 ± 6.6	0.3 ± 0.1	2.8 ± 0.8	20.3 ± 5.5	8.1 ± 2.3
mis-ID Z	0.1 ± 0.0	5.1 ± 2.6	7.7 ± 3.9	1.1 ± 0.6	0.0 ± 0.0	2.1 ± 1.0	5.2 ± 2.6	3.0 ± 1.5
Total Bkg.	46.2 ± 8.6	75.2 ± 12.4	309.2 ± 47.4	56.1 ± 8.6	13.6 ± 2.3	23.6 ± 3.5	63.5 ± 9.5	19.9 ± 3.2
$ZH(120)$ GeV/c^2	1.1 ± 0.1	1.1 ± 0.1	1.6 ± 0.2	0.3 ± 0.03	0.2 ± 0.04	0.2 ± 0.04	0.3 ± 0.1	0.1 ± 0.01
Data	45	83	352	66	16	23	59	23

TABLE IV: Comparison of the expected mean event totals for background and ZH signal with the observed number of data events for the $ZH \to e^+e^- + b\bar{b}$ channels. The totals are for full event selection, and uncertainties are systematic.

	–Two Jets–				–Three Jets–			
Process	TT	TL	Tx	LL	TT	TL	Tx	LL
$t\bar{t}$	20.8 ± 3.1	22.1 ± 3.1	30.4 ± 3.9	5.7 ± 0.8	6.4 ± 1.2	7.4 ± 1.2	10.4 ± 1.5	2.4 ± 0.4
Diboson	3.8 ± 0.6	5.1 ± 0.7	15.1 ± 1.5	3.0 ± 0.4	0.6 ± 0.1	0.9 ± 0.2	2.3 ± 0.3	0.8 ± 0.1
$Z + b\bar{b}$	15.0 ± 6.3	21.0 ± 8.8	64.4 ± 27.0	7.7 ± 3.2	3.5 ± 1.5	5.2 ± 2.4	11.3 ± 5.0	2.3 ± 1.1
$Z + c\bar{c}$	1.0 ± 0.4	4.6 ± 2.0	30.0 ± 12.6	6.3 ± 2.6	0.4 ± 0.2	1.5 ± 0.7	5.8 ± 2.5	1.9 ± 0.8
$Z + l.f.$	0.6 ± 0.3	6.2 ± 1.5	91.7 ± 20.2	19.4 ± 4.5	0.3 ± 0.1	2.2 ± 0.6	15.3 ± 4.0	6.3 ± 1.7
mis-ID Z	1.0 ± 0.1	0.0 ± 0.0	10.0 ± 0.5	1.0 ± 0.1	1.0 ± 0.1	8.0 ± 0.4	8.0 ± 0.4	5.0 ± 0.3
Total Bkg.	42.3 ± 7.1	58.9 ± 9.7	241.5 ± 36.3	43.0 ± 6.2	12.2 ± 1.9	25.2 ± 2.8	53.0 ± 7.0	18.8 ± 2.2
$ZH(120)$ GeV/c^2	0.9 ± 0.1	0.9 ± 0.1	1.4 ± 0.1	0.3 ± 0.03	0.2 ± 0.03	0.2 ± 0.04	0.2 ± 0.05	0.1 ± 0.01
Data	41	69	273	51	15	24	46	25

TABLE V: Comparison of the expected mean event totals for background and ZH signal with the observed number of data events for the $ZH \to \mu^+\mu^- + b\bar{b}$ channels. The totals are for full event selection, and uncertainties are systematic.

M_H (GeV/c^2)	Obs./SM	-2 σ/SM	-1 σ/SM	Med. Exp./SM	+1 σ/SM	+2 σ/SM
90	1.0	1.0	1.4	1.9	2.8	3.8
95	1.2	1.0	1.4	2.1	3.0	4.5
100	1.8	1.0	1.4	2.1	3.0	4.2
105	2.3	1.1	1.5	2.2	3.1	4.4
110	3.0	1.2	1.6	2.4	3.4	4.8
115	4.7	1.4	1.8	2.6	3.7	5.3
120	5.7	1.5	2.1	3.1	4.4	6.3
125	7.2	1.9	2.5	3.6	5.2	7.4
130	10.8	2.5	3.3	4.8	7.0	10.1
135	15.0	3.2	4.3	6.3	9.1	12.6
140	19.1	4.4	6.3	8.8	12.9	18.7
145	21.7	6.7	9.2	13.3	19.5	27.1
150	36.5	10.7	15.0	21.3	30.4	44.6

TABLE VI: The 95% CL upper limits on the ZH production rate expressed as a factor on $\sigma_{ZH} \times BR(H \to b\bar{b})$. The observed limits are obtain using CDF II data, while the median, -2,-1,+1, and +2 are obtained from the distribution of upper limits obtained in background-only pseudo-experiments.

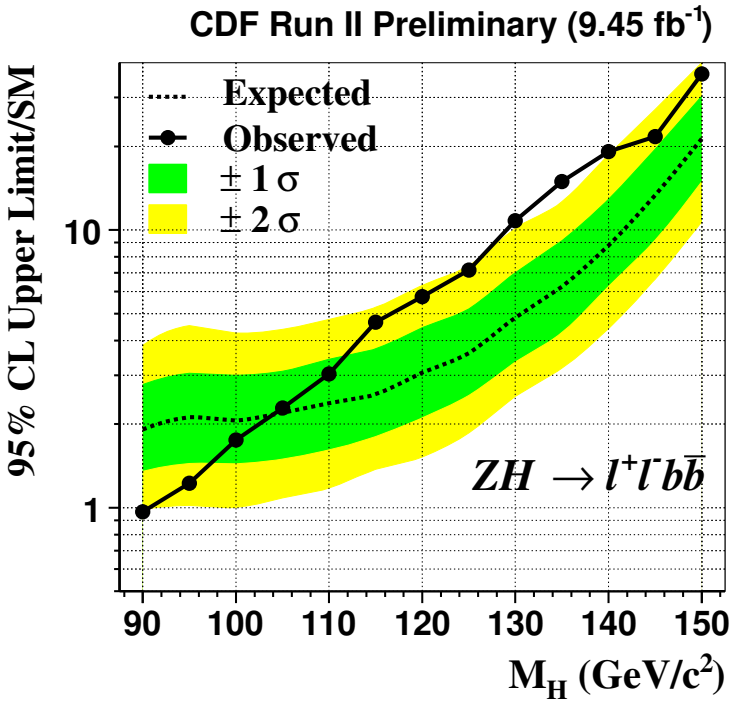

FIG. 7: The 95% CL upper limits on the ZH production rate expressed as a factor on $\sigma_{ZH} \times BR(H \to b\bar{b})$. The observed limits are obtain using CDF II data, while the median, -2,-1,+1, and +2 are obtained from the distribution of upper limits obtained in background-only pseudo-experiments.

[1] Higgs, P., Phys. Rev. Lett. **13** 508 (1964).
[2] Guralnik, G. S., *et. al.*, Phys. Rev. Lett. **13** 585 (1964).
[3] Englert, F. and R. Brout, Phys. Rev. Lett. **13** 321 (1964).
[4] Baak, M., *et. al.*, arXiv:1107.0975v1 [hep-ph] (2011)
[5] The LEP Electroweak Working Group. `http://lepewwg.web.cern.ch/LEPEWWG/`.
[6] CDF, D0, and the TEVNPHWG, arXiv:1107.5518v2 [hep-ex] (2011).
[7] CMS Collaboration, arXiv:1202.1488 [hep-ex] (2012).
[8] ATLAS Collaboration, arXiv:1202.1408 [hep-ex] (2012).
[9] Strange, A., *et. al.*, Phys. Rev. D **49** 1354 (1994).
[10] T. Aaltonen, (CDF Collaboration) Phys. Rev. Lett. **105** 251802 (2010).
[11] S. Lockwitz, Ph.D. thesis, Yale University (2011), FERMILAB-THESIS-2012-02.
[12] J. Pilot, Ph.D. thesis, The Ohio State University (2011), FERMILAB-THESIS-2011-42.
[13] Acosta, D., (CDF Collaboration), Phys. Rev. D. **71**, 032001 (2005).
[14] We use a cylindrical coordinate system with z along the proton beam direction, r the perpendicular radius from the central axis of the detector, and ϕ the aximuthal angle. for θ, the polar angle from the proton beam, we define η = -ln tan (θ/2). P_T refers to transverse momentum, while E_T denotes transverse energy.
[15] The missing E_T ($\vec{\not\!\!E}_T$) is defined by the sum over calorimeter towers: $\vec{\not\!\!E}_T = -\sum_i E_T^i \hat{n}_i$, where i = calorimeter tower number with $|\eta| < 3.6$, $\hat{n}_i$ is a unit vector perpendicular to the beam axis and pointing at the ith calorimeter tower. We also define $\not\!\!E_T = |\vec{\not\!\!E}_T|$.
[16] Blazey, G.C. and Flaugher, B.L., Ann. Rev. Nucl. Part. Sci. **49** 633-685 (1999).
[17] CDF Collaboration Note **10803**.
[18] Mangano, M., *et al.*, J. High Energy Phys. **07** 001 (2003).
[19] Sjöstrand, T., *et al.*, Comput. Phys. Commun. **135** 238 2001.
[20] CDF Collaboration Note **10804**.
[21] We define dijet mass resolution as the standard deviation of the dijet mass distribution divided by its mean.
[22] We define $\Delta R(x_i,\ x_j)$ as $\sqrt{((\eta_i - \eta_j)^2 + (\phi_i - \phi_j)^2}$).
[23] We define H_T as the sum of scalars $\not\!\!E_T$+ jet 1 E_T + jet 2 E_T + lepton 1 E_T + lepton 2 E_T.
[24] We define θ^* as the angle between the Z boson candidate and the proton beam direction in the zero momentum frame.
[25] CDF Collaboration Note **7816**.
[26] Junk, T., Nucl. Instrum. Meth. **A434** 435 (1999).

X. APPENDIX : SYSTEMATICS

TABLE VII: Systematic uncertainties on the signal and background contributions for tight double tag (TT), single tight plus single loose (TL), single tag (Tx), and loose double tag (LL) channels. Systematic uncertainties are listed by name. Separate analysis channels are defined by the Z boson decay mode ($Z \to e^+e^-$, $Z \to \mu^+\mu^-$), and by the number of jets. Systematic uncertainties for ZH shown in this table are obtained for $m_H = 115$ GeV/c^2. Uncertainties are relative, in percent, and are symmetric unless otherwise indicated. The jet energy scale uncertainties (JES) include a shape component.

CDF: tight double tag (TT) $ZH \to \ell^+\ell^- b\bar{b}$ channel relative uncertainties (%)

Contribution	Mis-ID Z	$t\bar{t}$	WW	WZ	ZZ	$Z + c\bar{c}$	$Z + b\bar{b}$	Mistags	ZH
Luminosity ($\sigma_{\rm inel}(p\bar{p})$)		3.8	3.8	3.8	3.8	3.8	3.8		3.8
Luminosity Monitor		4.4	4.4	4.4	4.4	4.4	4.4		4.4
Lepton ID		1	1	1	1	1	1		1
Lepton Energy Scale		1.5	1.5	1.5	1.5	1.5	1.5		1.5
Fake $Z \to e^+e^-$	50								
Fake $Z \to \mu^+\mu^-$	5								
Tight Mistag Rate								40	
Loose Mistag Rate									
JES [e^+e^-, 2 jet]		$^{+0.8}_{-0.7}$	$^{+14.4}_{-13.2}$	$^{+6.2}_{-6.2}$	$^{+8.2}_{-8.3}$	$^{+5.6}_{-5.6}$	$^{+8.1}_{-7.9}$	$^{+10.4}_{-10.4}$	$^{+3.6}_{-4.2}$
JES [e^+e^-, 3 jet]		$^{+8.3}_{-8.2}$	$^{-0.7}_{+1.7}$	$^{-4.2}_{+4.3}$	$^{+14.4}_{-13.3}$	$^{+10.6}_{-10.5}$	$^{+13.2}_{-13.2}$	$^{+12.4}_{-12.4}$	$^{+15.1}_{-14.9}$
JES [$\mu^+\mu^-$, 2 jet]		$^{+1.0}_{-0.9}$	$^{+5.4}_{+2.1}$	$^{+13.4}_{-13.4}$	$^{+7.7}_{-7.7}$	$^{-1.5}_{+1.5}$	$^{+8.2}_{-8.2}$	$^{+5.7}_{-5.8}$	$^{+3.1}_{-3.5}$
JES [$\mu^+\mu^-$, 3 jet]		$^{+9.3}_{-9.1}$	$^{+3.9}_{-3.0}$	$^{+4.8}_{-5.7}$	$^{+15.5}_{-15.5}$	$^{+7.3}_{-7.3}$	$^{+14.2}_{-14.5}$	$^{+20.5}_{-18.0}$	$^{+12.5}_{-13.3}$
Tight b-tag Rate		7.8	7.8	7.8	7.8	7.8	7.8		7.8
Loose b-tag Rate									
$t\bar{t}$ Cross Section		10							
Diboson Cross Section			6	6	6				
Z+HF Cross Section						40	40		
ZH Cross Section									5
ISR/FSR									5.5–7.6
Electron Trigger Eff.		1	1	1	1	1	1		1
Muon Trigger Eff.		5	5	5	5	5	5		5

CDF: single tight + single loose (TL) $ZH \to \ell^+\ell^- b\bar{b}$ channel relative uncertainties (%)

Contribution	Mis-ID Z	$t\bar{t}$	WW	WZ	ZZ	$Z + c\bar{c}$	$Z + b\bar{b}$	Mistags	ZH
Luminosity ($\sigma_{\rm inel}(p\bar{p})$)		3.8	3.8	3.8	3.8	3.8	3.8		3.8
Luminosity Monitor		4.4	4.4	4.4	4.4	4.4	4.4		4.4
Lepton ID		1	1	1	1	1	1		1
Lepton Energy Scale		1.5	1.5	1.5	1.5	1.5	1.5		1.5
Fake $Z \to e^+e^-$	50								
Fake $Z \to \mu^+\mu^-$	5								
Tight Mistag Rate								19	
Loose Mistag Rate								10	
JES [e^+e^-, 2 jet]		$^{+0.9}_{-1.0}$	$^{+13.0}_{-12.6}$	$^{+9.3}_{-9.4}$	$^{+10.3}_{-10.2}$	$^{+10.3}_{-10.3}$	$^{+8.9}_{-9.3}$	$^{+10.4}_{-10.4}$	$^{+4.0}_{-4.2}$
JES [e^+e^-, 3 jet]		$^{+6.9}_{-7.0}$	$^{+10.3}_{-8.3}$	$^{+16.2}_{-16.0}$	$^{+14.6}_{-14.5}$	$^{+22.8}_{-23.4}$	$^{+15.1}_{-15.2}$	$^{+18.5}_{-18.5}$	$^{+14.3}_{-14.4}$
JES [$\mu^+\mu^-$, 2 jet]		$^{+1.1}_{-1.1}$	$^{+3.7}_{1.8}$	$^{+6.5}_{-6.5}$	$^{+7.5}_{-7.5}$	$^{+12.5}_{-12.4}$	$^{+10.1}_{-10.1}$	$^{+11.0}_{-11.0}$	$^{+4.0}_{-4.1}$
JES [$\mu^+\mu^-$, 3 jet]		$^{+8.0}_{-8.0}$	$^{+2.0}_{-1.6}$	$^{+14.4}_{-14.5}$	$^{+24.1}_{-24.1}$	$^{+16.0}_{-14.7}$	$^{+17.5}_{-17.6}$	$^{+14.3}_{-14.2}$	$^{+13.1}_{-14.0}$
Tight b-tag Rate		3.9	3.9	3.9	3.9	3.9	3.9		3.9
Loose b-tag Rate		3.2	3.2	3.2	3.2	3.2	3.2		3.2
$t\bar{t}$ Cross Section		10							
Diboson Cross Section			6	6	6				
Z+HF Cross Section						40	40		
ZH Cross Section									5
ISR/FSR									3.4–7.0
Electron Trigger Eff.		1	1	1	1	1	1		1
Muon Trigger Eff.		5	5	5	5	5	5		5

CDF: single tight (Tx) $ZH \to \ell^+\ell^- b\bar{b}$ channel relative uncertainties (%)

Contribution	Mis-ID Z	$t\bar{t}$	WW	WZ	ZZ	$Z + c\bar{c}$	$Z + b\bar{b}$	Mistags	ZH
Luminosity ($\sigma_{\rm inel}(p\bar{p})$)		3.8	3.8	3.8	3.8	3.8	3.8		3.8
Luminosity Monitor		4.4	4.4	4.4	4.4	4.4	4.4		4.4
Lepton ID		1	1	1	1	1	1		1
Lepton Energy Scale		1.5	1.5	1.5	1.5	1.5	1.5		1.5
Fake $Z \to e^+e^-$	50								
Fake $Z \to \mu^+\mu^-$	5								
Tight Mistag Rate								19	
Loose Mistag Rate									
JES [e^+e^-, 2 jet]		$^{-0.3}_{+0.3}$	$^{+13.7}_{-13.5}$	$^{+8.5}_{-8.5}$	$^{+6.5}_{-6.3}$	$^{+13.2}_{-13.2}$	$^{+11.0}_{-11.1}$	$^{+12.0}_{-12.0}$	$^{+3.5}_{-3.8}$
JES [e^+e^-, 3 jet]		$^{+7.1}_{-7.1}$	$^{+8.9}_{-8.2}$	$^{+17.0}_{-17.0}$	$^{+15.4}_{-15.4}$	$^{+16.4}_{-16.4}$	$^{+15.8}_{-15.9}$	$^{+18.6}_{-18.5}$	$^{+15.4}_{-15.7}$
JES [$\mu^+\mu^-$, 2 jet]		$^{+0.6}_{-0.7}$	$^{+3.9}_{-3.3}$	$^{+8.6}_{-8.6}$	$^{+7.6}_{-7.7}$	$^{+10.2}_{-10.5}$	$^{+9.3}_{-9.3}$	$^{+11.1}_{-11.1}$	$^{+3.4}_{-3.7}$
JES [$\mu^+\mu^-$, 3 jet]		$^{+5.5}_{-5.5}$	$^{+5.7}_{-1.9}$	$^{+16.6}_{-16.6}$	$^{+16.8}_{-16.8}$	$^{+16.1}_{-16.2}$	$^{+16.1}_{-16.2}$	$^{+17.5}_{-17.5}$	$^{+13.8}_{-13.9}$
Tight b-tag Rate		3.9	3.9	3.9	3.9	3.9	3.9		3.9
Loose b-tag Rate									
$t\bar{t}$ Cross Section		10							
Diboson Cross Section			6	6	6				
Z+HF Cross Section						40	40		
ZH Cross Section									5
ISR/FSR									0.9–12.8
Electron Trigger Eff.		1	1	1	1	1	1		1
Muon Trigger Eff.		5	5	5	5	5	5		5

CDF: loose double tag (LL) $ZH \to \ell^+\ell^- b\bar{b}$ channel relative uncertainties (%)

Contribution	Mis-ID Z	$t\bar{t}$	WW	WZ	ZZ	$Z + c\bar{c}$	$Z + b\bar{b}$	Mistags	ZH
Luminosity ($\sigma_{\rm inel}(p\bar{p})$)		3.8	3.8	3.8	3.8	3.8	3.8		3.8
Luminosity Monitor		4.4	4.4	4.4	4.4	4.4	4.4		4.4
Lepton ID		1	1	1	1	1	1		1
Lepton Energy Scale		1.5	1.5	1.5	1.5	1.5	1.5		1.5
Fake $Z \to e^+e^-$	50								
Fake $Z \to \mu^+\mu^-$	5								
Tight Mistag Rate									
Loose Mistag Rate								20	
JES [e^+e^-, 2 jet]		$^{+0.5}_{-0.5}$	$^{+7.5}_{-4.8}$	$^{+8.6}_{-8.7}$	$^{+9.0}_{-8.9}$	$^{+10.0}_{-9.3}$	$^{+11.3}_{-11.0}$	$^{+12.5}_{-12.5}$	$^{+4.0}_{-4.4}$
JES [e^+e^-, 3 jet]		$^{+8.6}_{-8.6}$	$^{+32.9}_{-29.5}$	$^{+14.6}_{-14.9}$	$^{+16.5}_{-15.2}$	$^{+20.8}_{-20.8}$	$^{+17.8}_{-17.9}$	$^{+18.9}_{-19.0}$	$^{+14.6}_{-15.4}$
JES [$\mu^+\mu^-$, 2 jet]		$^{+2.5}_{-2.5}$	$^{+4.5}_{-3.0}$	$^{+6.7}_{-6.7}$	$^{+10.2}_{-9.9}$	$^{+9.2}_{-9.3}$	$^{+7.7}_{-7.6}$	$^{+11.5}_{-11.5}$	$^{+3.9}_{-4.3}$
JES [$\mu^+\mu^-$, 3 jet]		$^{+9.2}_{-9.2}$	$^{+13.4}_{-10.4}$	$^{+14.1}_{-14.1}$	$^{+16.6}_{-16.6}$	$^{+14.7}_{-14.7}$	$^{+16.8}_{-16.9}$	$^{+17.5}_{-17.5}$	$^{+11.6}_{-12.2}$
Tight b-tag Rate									
Loose b-tag Rate		6.3	6.3	6.3	6.3	6.3	6.3		6.3
$t\bar{t}$ Cross Section		10							
Diboson Cross Section			6	6	6				
Z+HF Cross Section						40	40		
ZH Cross Section									5
ISR/FSR									3.1–15.2
Electron Trigger Eff.		1	1	1	1	1	1		1
Muon Trigger Eff.		5	5	5	5	5	5		5